Multiphase alternated slug flows: conditions to avoid coalescence and characterization of mass transfer between droplets

Camille Méhault, Laurent Vanoye, Régis Philippe, Claude de Bellefon

Multiphase alternated slug flows: conditions to avoid coalescence and characterization of mass transfer between droplets.

Camille Méhault, Laurent Vanoye, Régis Philippe, Claude de Bellefon*

Univ. Lyon, Laboratoire de Génie des Procédés Catalytiques, UMR 5285 CNRS, CPE Lyon, Université Claude Bernard Lyon 1, 43 Boulevard du 11 Novembre 1918, 69100 Villeurbanne, France.

**Corresponding author: claude.debellefon@lgpc.cpe.fr*

Abstract: Alternated slug flow in capillaries is an efficient way to separate droplets with different compositions for applications in various fields. This paper describes how to solve the main issue, i.e. droplets coalescence, by using a gas bubble as a separator and demonstrates quantitatively how the mass transfer between resulting liquid-(gas-liquid)-liquid flow is negligibly impacted by the gas bubble size distribution generated. Thus residence time of up to 30 min could be achieved avoiding coalescence. The conditions to generate and maintain the alternated flow such as the superficial velocities, viscosities and surface tensions, are provided. The mechanism for mass transfer between droplets is shown to occur mainly through the film at the wall of the capillaries explaining the negligible impact of the gas. Mastering such alternated slug flow opens the door for many applications requiring compartmentation of several reactions.

1. Introduction

Structuring the reaction media is a way for process intensification and reliable solutions such as monolithic reactors are today applied [1]. Such reactors are mostly operated with gas-liquid media, a solid being possibly coated at the wall of the monolith structure, with a G/L segmented flow providing many advantages and has been thoroughly examined [2]. Indeed, segmented flow provides narrow residence time distribution, high surface to volume ratio, increased mixing by the presence of recirculation loops which enhances the mass transfer [3]. Nowadays an increasing amount of studies also include more complex multiphasic flow such as G/L/L [4]–[6], G/L/S [7]–[11] or L/L/S [12], [13]. Multiphasic flows have been investigated as part of specific applications including G/L reaction coupled with L/L extraction [4], heterogeneous catalysis [7] and production of solid materials [8]. Although it is very clear that segmented flow could potentially operate with a very large diversity of physical phases, the property of segmented flow to tune and use coalescence has seldom been used for reacting systems. With segmented flow, coalescence of droplets could be used to trigger a reaction, or could be avoided if required. Thus, one can take advantages of this property to perform cascades reactions in a single reactor, i.e. in one-flow, including with non-compatible reactions.

Using such spatial confinement is a rather new concept called compartmentalization. It has been applied with mitigated results in stirred tank reactors for reactions involving solid catalysts which were maintained in different zones of the reactor [14], [15]. In such reactors, operating with fluids and/or powder catalysts is obviously more difficult since coalescence will occur leading to losing compartmentalization.

Although most applications in microfluidic systems revolve around single step synthesis, a growing number of studies have investigated multi-step reactions with promising results [16]–[18]. The approach is to connect several flow reactors in series without having to isolate reactive intermediates. The reaction steps that are performed in different reactors are often not compatible with each other due to incompatible media or operating conditions (temperature, residence time, pressure), thus calling for separation units between the reactors. This work proposes to go one step further into process

intensification by using compartmentalization, to perform multistep reactions inside just one reactor. One advantage of this technique is to reduce the number of operating units in the global process. The proposed versatile tool is particularly suited for multi-step reactions occurring in incompatible but miscible reaction media with compatible operating conditions like temperature and residence time.

To compartmentalize two miscible phases inside a flow reactor, the idea is to generate two droplets respectively containing the two reactive phases separated by a non-miscible and inert liquid media carrier. One of the difficulties is to inject both droplets in the system without coalescence occurring. The formation of this L/L/L segmented flow, called the alternated segmented flow (ASF), has been investigated in the literature in small square microchannel (internal diameter <500 μm) [19]–[23] with the generation of different flow regimes (merging, alternating, small droplets and laminar) depending on the operating conditions [19], [20]. Very recently, a device to generate alternated segmented flow in circular PFA tubing (i.d of 2.18mm) using a system of valves to control the phase injection has been developed [24]. This work offers a simpler way to generate alternated segmented flow without the need of active control at the injection. Until now, the alternated segmented flow has found only limited applications. Among existing applications, a device that generates alternating droplets which allows to control their coalescence using a specific channel geometry for the synthesis of CdS nanoparticles has been described [22]. In another application, alternated segmented flow was used to screen conditions for protein crystallization [20].

However, in both applications, the residence times used were very short (typically < 1s) and no information was given on the outcome of the alternated segmented flow (i.e. after less than a few seconds of residence time). Also, the size and shape of the channels were less appropriate compared to flow chemistry tools that generally use millimetre sizes circular tubes. Last but not least, the nature of the materials, could it be the wall of the channel, PDMS in the previous studies, and the transport liquids were adapted to fit specific viscosities and surface tensions by using surfactants.

The objective of this work is to provide a tool to perform multistep cascade reactions that are not compatible. For such applications, it is mandatory to maintain the alternated segmented flow for a

relatively long residence time, i.e. more than minutes. Therefore, this work will first tackle the challenge to generate and stabilise the alternated flow along the reaction channel, avoiding droplet coalescence and then to assess the mass transfer between the two droplets.

2. Materials and methods

2.1. Experimental set up

The experimental set up is illustrated in Figure 1 (a). Three syringe pumps (Harvard Apparatus PHD 4400) control precisely the mass flow-rates of each liquid phase without pressure fluctuations (flow range from 0.05 to 1.5 mL/min). The two dispersed phases and the continuous phases are injected into a commercially available cross junction (Upchurch Scientific, ¼-28 flat bottom PEEK with an internal

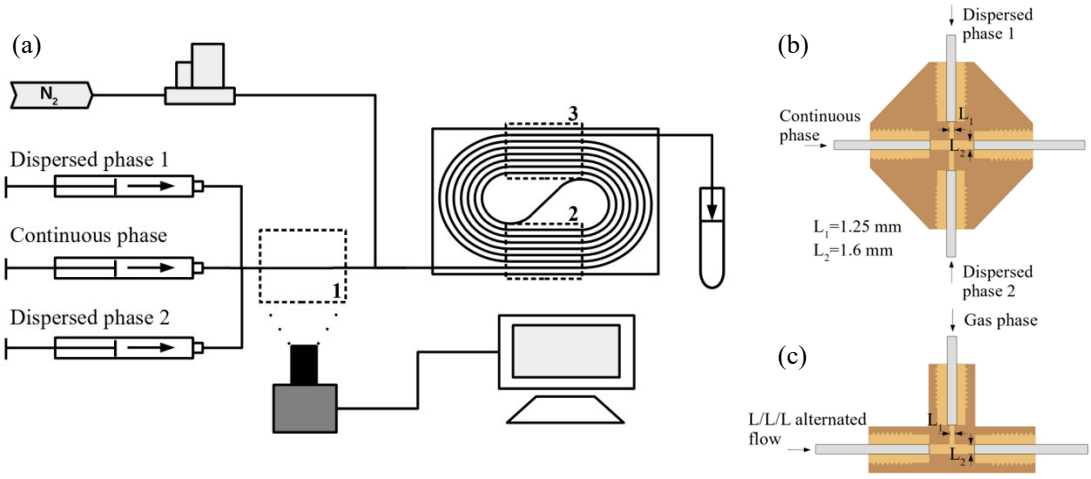

Fig. 1: (a) Experimental set up used for hydrodynamic and mass transfer experiments. The visualisation zones are represented by the dashed line boxes. (b) Geometry of the cross injector, (c) Geometry of the T iniector

diameter of 1.25 mm) to form a L/L/L segmented flow. The main channel of the cross injector was resized to obtain a channel diameter of 1.6 mm corresponding to the PFA tubing diameter (see Fig. 1 (b)).

For the majority of the experiments an injection of inert gas (N_2) was made after the cross junction using a mass flow controller (Analyt-MTC, Serie 358, 0-2mL/min).The L/L/L segmented flow and the gas are injected into a T junction (Upchurch Scientific, ¼-28 flat bottom PEEK with an internal

diameter of 1.25 mm) to form the G/L/L/L segmented flow. The main channel of the T injector was resized to obtain a channel diameter of 1.6 mm (see Fig. 1 (c)). A high speed colour camera (Basler ace U with a maximum acquisition speed of 75 images/s) equipped with an objective for close up visualization (Opto 1,0x 043-216250) and one for larger view of the full coiled reactor (Fujinon lens CF50ZA-1S) is used to capture videos of the flow after the injection and further down the reactor. A coiled reactor with a special compact arrangement was added to study the outcome of the alternated flow for long residence time. Details of the design were published previously [6]. The reactor is made of PFA tubing (1.6 mm i.d) and has a total length of 10 m. To ensure high-quality videos, the coiled reactor is placed inside a transparent visualisation PMMA box filled with deionized water that match with the refractive index of the PFA tubing, thus enabling reproducible optical conditions. The reactor is submitted to back illumination by a LED panel (Just Normlicht, Classic Line) which provides a uniform lightning for every channel.

2.2. Hydrodynamic experiments

In a typical hydrodynamic experiment, the continuous organic phase and the aqueous dispersed phases are placed inside the syringes and pushed into the injection system at the desired flow rates. The stability of the flow is observed directly after the injection as well as further down the coiled reactor at several residence times. The properties of the fluids used in the study are presented in Table 1. Dodecane (Sigma Aldrich, >99%), squalane (Sigma Aldrich, 96%) and silicon oil (CALSIL IP 20) were tested as continuous phases. Water, water/glycerol, water/methanol and water/DMSO mixtures were employed as the dispersed phases. Red and blue dyes were added to the two dispersed phases to facilitate the flow visualisation. No surfactants were added in contrast to other works.

Table 1: Properties of the liquid phases used in the hydrodynamic study.

Phase	Composition	Viscosity[a] cP	Surface tension[b] mN/m
Continuous	Squalane	35.6	29 [c]
	Dodecane	1.36	26
	Silicon oil	19	20.6
Dispersed	Water	1	72
	Water/Methanol (1:1 vol)	1.5	33
	Water/DMSO (1 :1 vol)	2.9	59.6
	Water/DMSO (1:8 vol)	2.7	47.7
	Water/glycerol (1:3 mass)	35.5	67

[a] At 20°C, [b] with air at 20°C, [c] This value is for squalene, that for squalene was not found.

2.3. Mass transfer experiments

The mass transfer between the two aqueous droplets was investigated using the acid-base reaction between sodium hydroxide and acetic acid. A solution of sodium hydroxide ($C_{OH^-}^0$=1.3.10^{-4}mol/L, pH=10.13) with a colour indicator (phenolphthalein) was injected as the first dispersed phase (aq1). The second dispersed phase (aq2) is an acetic acid solution with helianthine as colour indicator. Squalane is used as the continuous phase. In most experiments, N_2 is added as separator between the two droplets to obtain a stable alternated segmented flow. N_2 being poorly soluble in liquids, the gas mass flow inside the reactor is taken as the same at the reactor inlet. During the experiments, the colour of the basic droplet will gradually change from purple to colourless. The discolouration indicates the transfer of acetic acid from the acid droplet to the basic droplet where it is neutralized. Videos of the alternated segmented flow were recorded at different residence times by changing the camera position above the coiled reactor.

2.4. Image analysis

To quantify the discolouration of the basic droplet, a colorimetric method by image analysis using a Matlab® routine was developed. As a reminder, a colour image is composed of three matrices in the RGB space corresponding to the blue, green and red components. Image analysis was carried out on

the green matrix where the observed changes are more sensible (see Fig. 2 (b)). Detection of the basic droplet was made manually by selecting a polygon following the outline of the droplet (see Fig.2 (c)).

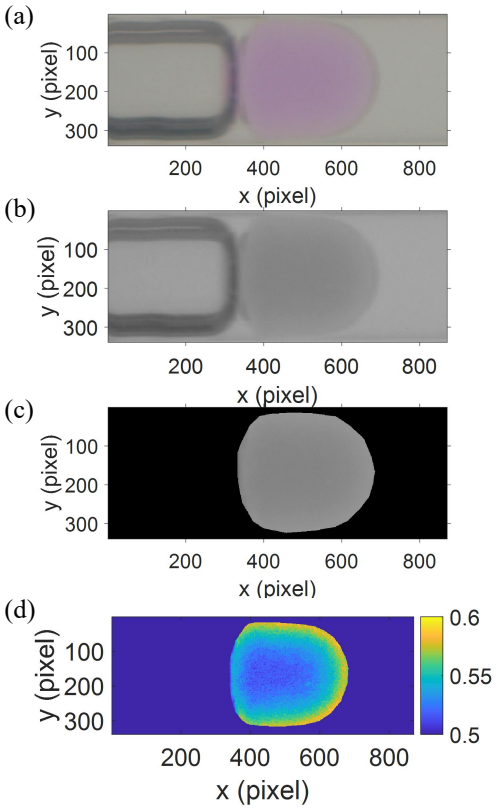

Fig. 2: Image analysis (a) Original image, (b) Green component of the RGB image, (c) Manual detection of basic droplet, (d) Green matrix with scaled colour.

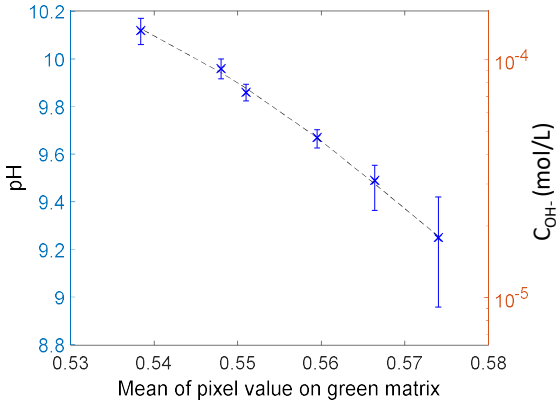

Fig. 3: Calibration curve between the OH^- concentration of the basic droplet and mean of pixel values taken for the green component of the original RGB image.

The pH of the basic aqueous droplet (aq1) was then correlated to the mean value of pixels composing the selected polygon. For this, a calibration curve (see Fig. 3) was made by using several solutions of sodium hydroxide with known pH (9.25<pH<10.13). The solutions of sodium hydroxide were placed inside one syringe whereas the other syringe contained deionized water (18 MΩ). Both dispersed phases (water and sodium hydroxide solution), squalane and N_2 were then injected to form the alternated segmented flow. For each sodium hydroxide solution, videos were recorded and about 8 pictures of the basic droplet were analysed to obtain an average. The calibration curve was interpolated by a second order polynomial function.

The remaining concentration of sodium hydroxide $C_{OH-,aq1}$ can then be obtained using the calibration curve and the conversion X with regards to the hydroxide ions can be calculated as:

$$X = \frac{{C_{OH-}}^{0} - C_{OH-,aq1}}{{C_{OH}}^{0}} \quad (1)$$

The rate of acetic acid mass transfer can be estimated as the rate of OH^- consumption. It is however essential to mention that the calibration curve will depend on the experimental conditions especially the light intensity.

2.5. Verification of droplet homogeneity

In order to calculate the OH^- conversion with the colorimetric method, it is necessary to verify that the concentration of OH^- is homogeneous over the whole droplet. For this, it is important to note that even for the calibration droplet (without acetic acid) the pixel values in the green matrix are not uniform over the entire droplet (see Fig. 2 (d)).

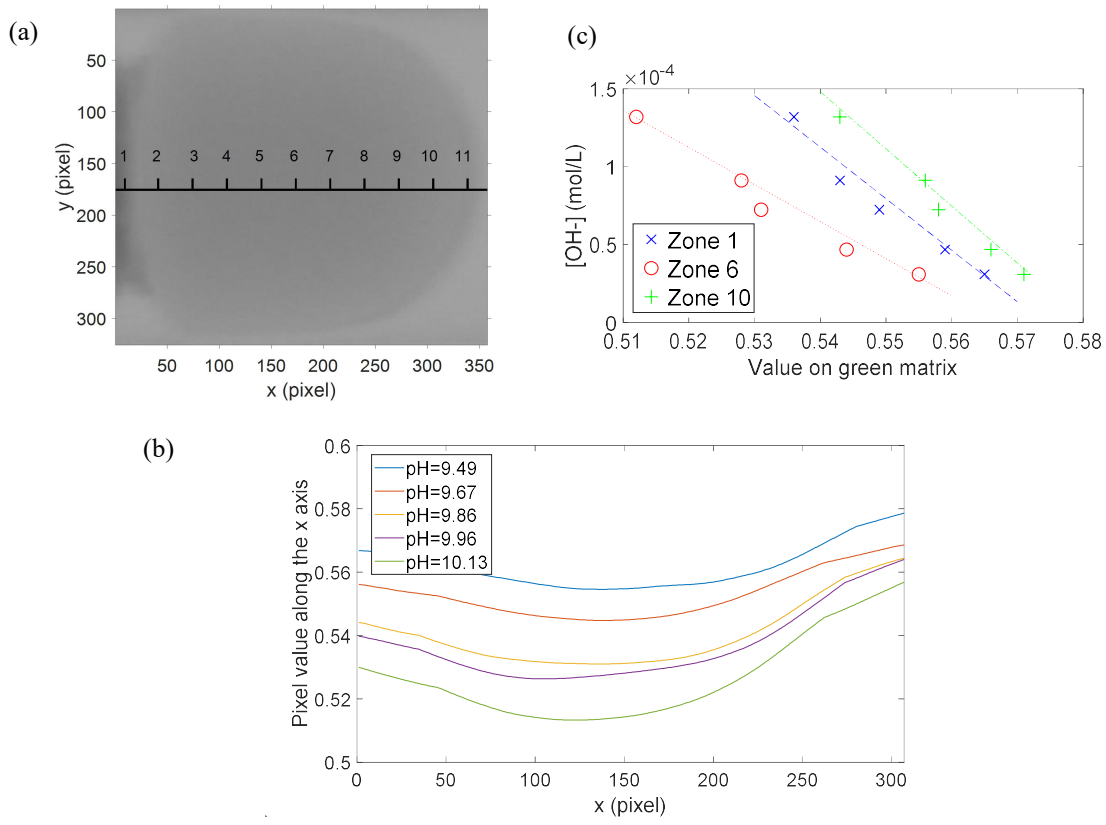

Fig. 4: Verification of concentration homogeneity in the basic droplet, (a) Segmentation of the x axis into 11 points (b) Pixel value along the x axis for the calibration solutions, (c) Calibration between the concentration of OH^- and the pixel value at different point in the x axis (three zones 1, 6 and 10 are given as an example, the full set of data is available in the ESI).

Due to the droplet 3D shape and the 2D images, an intensity gradient from the droplet centre to the droplet border was observed. To perform the homogeneity verification, the OH^- concentration is studied at different points in the horizontal x-axis represented in Fig. 4 (a). Along the x-axis, the pixel values formed an inverted bell-shaped curve for all calibration solutions (see Fig. 4 b)). For each point along the x-axis defined in Fig. 4 (a), the pixel values at the different OH^- concentrations were retrieved and correlated to the OH^- concentration using a linear approach as a first approximation (see Fig. 4 (c)). The calibration can be used to calculate the concentration of OH^- along the x axis. If the concentration is homogeneous, the calibration curve in Fig. 3 can be used to calculate the remaining OH^- concentration and thus the OH^- conversion. A summary of the Matlab® routine is represented in

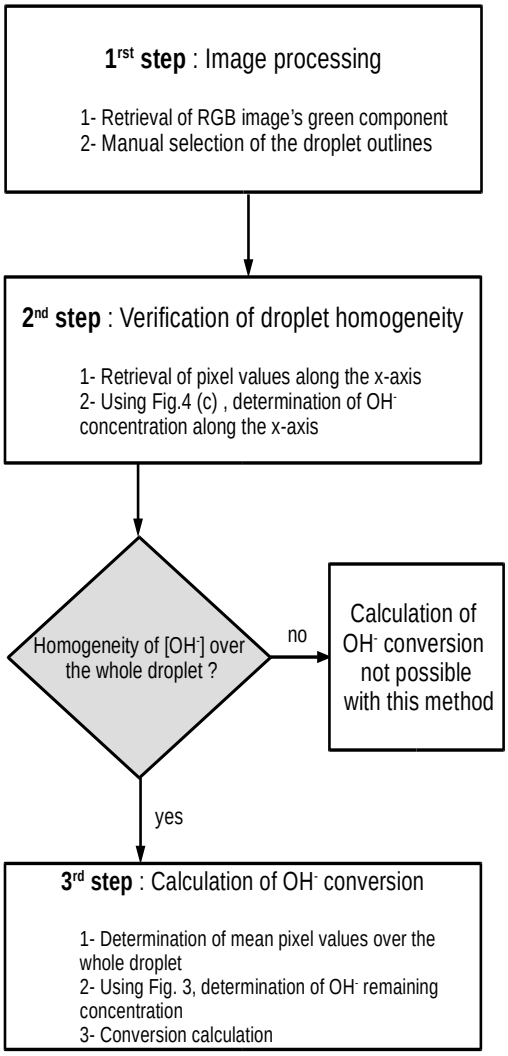

Fig. 5: Summary of Matlab® routine step for the image analysis.

Fig. 5. More details could be found in the ESI.

3. Results and discussion

3.1. Hydrodynamic study of the alternated segmented flow

Alternated segmented flow was obtained using the described experimental set up for specific experimental conditions which are presented in the following section.

3.1.1. Identification of flow regimes

In this section, experiments were made using squalane as the continuous phase and deionized water as the two dispersed phases in order to identify the correct operating window to obtain alternated flow with our system. As already successfully introduced for smaller channels with rectangular cross sections [20], the capillary number Ca and the total water fraction ε_{aq} are useful descriptors of the different flow regime frontiers (see Fig. 6 (a)). The capillary number is calculated as $Ca=U\mu_{squalane}/\gamma_{w/s}$ and the water fraction, ε_{aq}, is defined as:

$$\varepsilon_{aq} = \frac{Q_{aq1} + Q_{aq2}}{Q_{squalane} + Q_{aq1} + Q_{aq}} \quad (2)$$

This correlation implies the assumption of no slip velocity. Taking published correlations,[25], [26] and considering the range of Ca number in our experiments (i.e. $0.001 < Ca < 0.01$), the ratio S between the bubble velocity and the total superficial velocity is estimated in the range $0.02 < S < 0.12$ which supports the hypothesis of no slip velocity between phases. Three flow regimes were identified. At low capillary number ($Ca<0.002$) or high water fraction ($\varepsilon_{aq} >0.65$), the aqueous droplets directly coalesce at the injection (see Fig. 6 (b)). At higher capillary number ($Ca>0.002$) and intermediate water fraction ($0.2<\varepsilon_{aq}<0.65$), the desired

alternated segmented flow where droplets are successively formed was obtained (see Fig. 6 (d)). Thus coalescence could be avoided providing that a sufficient flow rate of squalane is injected. Illustrative pictures and videos of this phenomenon are provided in the ESI (Fig. S1 and corresponding videos 1 and 2). With a decrease of water fraction, smaller droplets with a length inferior to the channel diameter were observed (see Fig. 6 (c)). The regimes obtained are similar to those previously described [20] [19], with the exception of the laminar flow which is not observed in this study.

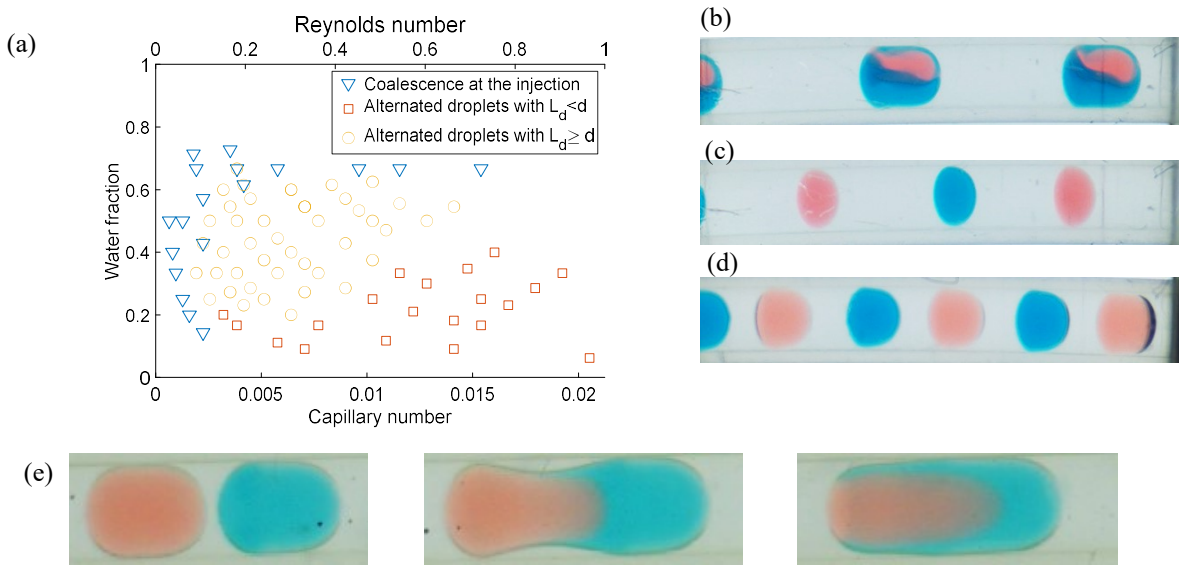

Fig. 6: (a) Cartography of flow regimes taken 2 cm after the cross junction as a function of the water fraction and the Capillary number using squalane as the continuous phase. Pictures of the corresponding flow regime are illustrated by (b) for the merging regime, (c) for the alternated segmented flow with small droplets and (d) for the alternated segmented flow L_d>d. (e) Fast coalescence of the aqueous droplet after the cross junction.

However after forming the alternated segmented flow, the droplets rapidly merge in the reactor (less than one minute of residence time) as shown in Fig. 6 (e).

This phenomenon is likely due to a slight variation in the drop size which results in small variation of the droplet velocity. Indeed, this work is performed under conditions between the segmented regime and the droplet flow regime. Under such condition, any decrease of the droplet volume will lead to a decrease of the droplet diameter. Such a smaller droplet will not “stick” to the stagnant film hence will likely have a slightly different velocity compared to the next droplet, which in turn will cause ultimately coalescence. The film of squalane between them will eventually break leading to coalescence [27]. More details on the droplet coalescence are presented in the ESI. As explained in

the introduction, no studies are available regarding the stabilisation of alternated segmented flow for the long residence time required by many chemical reactions while avoiding coalescence.

3.1.2. Stabilisation of alternated segmented flow

Experiments were made at a constant water fraction (ε_{aq} = 0.4) using squalane as the continuous phase and deionized water as the dispersed phases. Nitrogen is introduced into the system after the formation of the $L_{Aq1}/L_{Org}/L_{Aq2}$ alternated flow. For several squalane flow rates ($Q_{squalane}$) from 0.2 mL/min to 1 mL/min, the corresponding aqueous flow rates (Q_{aq1} and Q_{aq2}) were chosen to obtain a water fraction equal to 0.4 where the L/L/L alternated flow can be formed for a relatively large range of superficial velocity. For each triplet of flow rates, the gas flow rate (Q_{gas}) was varied from 0.1 to 1.2 mL/min. The

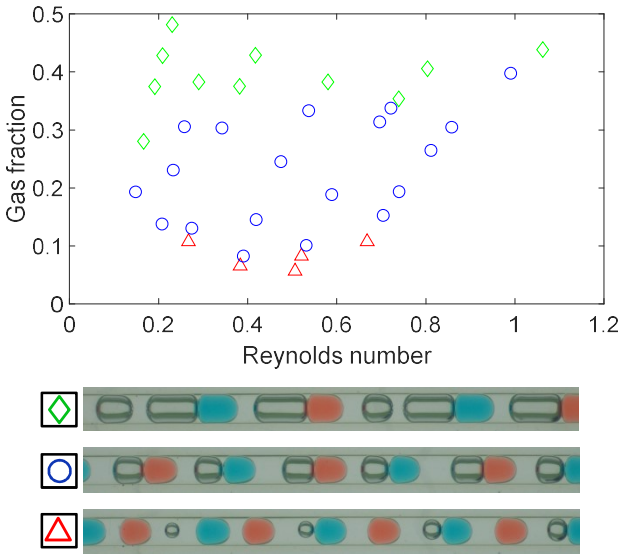

Fig. 7: Mapping of flow regimes with the addition of a N_2 gas phase at constant water fraction using squalane as the continuous phase and deionized water as dispersed phases.

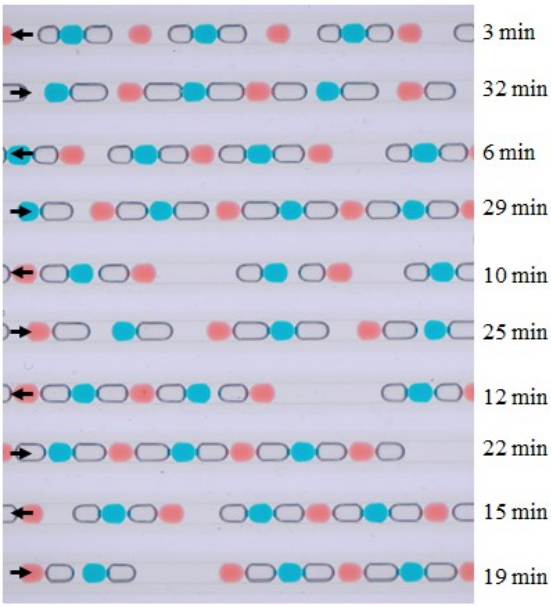

Fig. 8: Outcome of the G/L/L/L alternated flow for long residence times. The picture was taken in the visualization zone n°3. The residence time is given for each channel.

corresponding flow map (see Fig. 7) depicts the regimes obtained depending on the gas fraction, i.e. the ratio between Q_{gas} and the total flow rate, and the Reynolds number.

Three regimes were identified. At low gas fraction (ε_{N2} <0.1), where the bubble length is smaller than

the channel diameter, gas bubbles are inserted approximately every two aqueous droplets. At intermediate gas fraction, gas bubbles are injected between each droplet (See Fig. S2 and corresponding videos 3 in ESI). If the gas fraction increases even further, several gas bubbles can be injected between the aqueous droplets. Whenever there is a gas bubble between every aqueous droplet, coalescence between the two dispersed phases cannot happen since gas bubbles are very rigid and hardly breakable at such small scale. Even a small bubble (with a diameter significantly smaller than the channel diameter) can prevent the coalescence (see Fig S4 in the ESI). To be representative of various chemical applications, thirty minutes of residence time was therefore achieved in the 10 meter coiled reactor (see Fig. 8). It could be seen that the alternated segmented flow is preserved without coalescence even for long residence time (> 30 min) albeit with some irregularities in the squalane slug length. A view of the complete coiled reactor is given in the ESI as well as in the supplementary video (video 4).

3.1.3. Influence of fluid properties

The possibility of forming alternated segmented flow depends significantly on the properties of the liquid phases. Thus the generation of alternated segmented flow for various liquids was investigated (Table 2). For the continuous phase, the viscosity seems to play a major role in the formation of the alternated segmented flow. Using a less viscous alkane (dodecane), the formation of alternated segmented flow is no longer possible with our experimental set up. Using silicon oil which has an intermediate viscosity between dodecane and squalane, the formation of alternated segmented flow is still possible. For the dispersed phase, increasing the viscosity (using mixture of glycerol and water) doesn't change the experimental conditions to obtain the alternated segmented flow. However, decreasing the surface tension between both phases by adding methanol in the aqueous phase hinders the formation of alternated segmented flow. Note here that some surface tensions in Table 2 were estimated from published correlations.[28] Similarly, using a mixture of water/DMSO (1:8 vol), which has an intermediate surface tension, results in a reduction of the operating window. More details on the hydrodynamic study with water/DMSO mixtures are shown in the ESI. As a conclusion, the system

must be operated with continuous phase having viscosities above 19 cP and with surface tensions between the dispersed phase and the continuous phase greater than 30 mN/m.

Table 2: Formation of alternated segmented flow for different continuous and dispersed phases.

			Organic continuous phase [a]		
			Dodecane	Squalane	Silicon oil
		μ (cP)	1.36	35.59	19
Aqueous dispersed phase	μ (cP)	$\gamma_{i/air}$ (mN/m)	29	26	20.6
Water	1	72	46 -	43 +	51 +
Water/Methanol (1:1 vol)	1.5	33	7 -	4 -	12 [b]
Water/DMSO (1:1 vol)	2.9	59.6	30 -	33 +	39 [b]
Water/DMSO (1:8 vol)	2.7	47.7	22 -	19 0	27 [b]
Water/glycerol (1:3 mass)	35.5	67	41 -	38 +	46 [b]

[a] Symbol used: formation of alternated segmented flow is not possible (-), alternated segmented flow can be formed but with a reduced operating windows compared to the squalane/water system (0), alternated segmented flow can be generated (+). The values at the left of the symbols are the surface tension between the two phases. [b] Not investigated.

3.2. Mass transfer study between the two droplets

The purpose of this work is to introduce a tool to perform cascade reactions that are not compatible inside separated compartments (the two aqueous droplets). However during the cascade reaction, reactive intermediates need to transfer from one compartment to the other. The objective of this section is to study the mass transfer between the two aqueous droplets.

3.2.1. Influence of initial concentration of acetic acid

The concentration of acetic acid was varied in the range 0.02 M to 0.5 M and experiments were made at the—fixed volumetric flow rates ($Q_{squalane}$=0.3 mL/min, Q_{aq1}=0.12 mL/min, Q_{aq2}=0.12 mL/min and Q_{gas}=0.3 mL/min). Following the Matlab® routine described in Fig. 5, the homogeneity of OH^- concentration over the whole basic droplet was studied. At C_{AcOH}^0=0.5 M (see Fig. 9 (d)), a bell-shaped curve is obtained indicating that the OH^- concentration is not homogeneous along the x-axis.

At C_{AcOH}^0=0.25 M (see Fig. 9(c)), a bell-shaped curve is still observed but is less pronounced. With the decrease of the acetic acid concentration (C_{AcOH}^0=0.1 M and C_{AcOH}^0=0.05 M), no bell-shaped curve is observed and the OH^- concentration is approximately uniform along the x-axis (see Fig. 9 (a) and (b)). Therefore, for experiments using acetic acid concentration inferior or equal to 0.1 M, the OH^- concentration is assumed uniform in the whole droplet and the calibration curve previously determined (Fig. 3) can be used. With a higher acetic acid concentration, a gradient of OH^- concentration is observed indicating a possible transport limitation due to mixing (mainly by diffusion) inside the basic droplet.

For the experiments at initial concentration of acetic acid inferior or equal to 0.1M, the evolution of the conversion along the reactor for different acetic acid concentrations is represented in Fig. 10. An increase of the initial acetic acid concentration results in an increase of the apparent OH^- neutralization rate and therefore of the overall transport rate of acetic acid between the two aqueous droplets, r_{AcOH}. To globally characterize the transport of acetic acid, a global conductance K_{eff}, which describes the

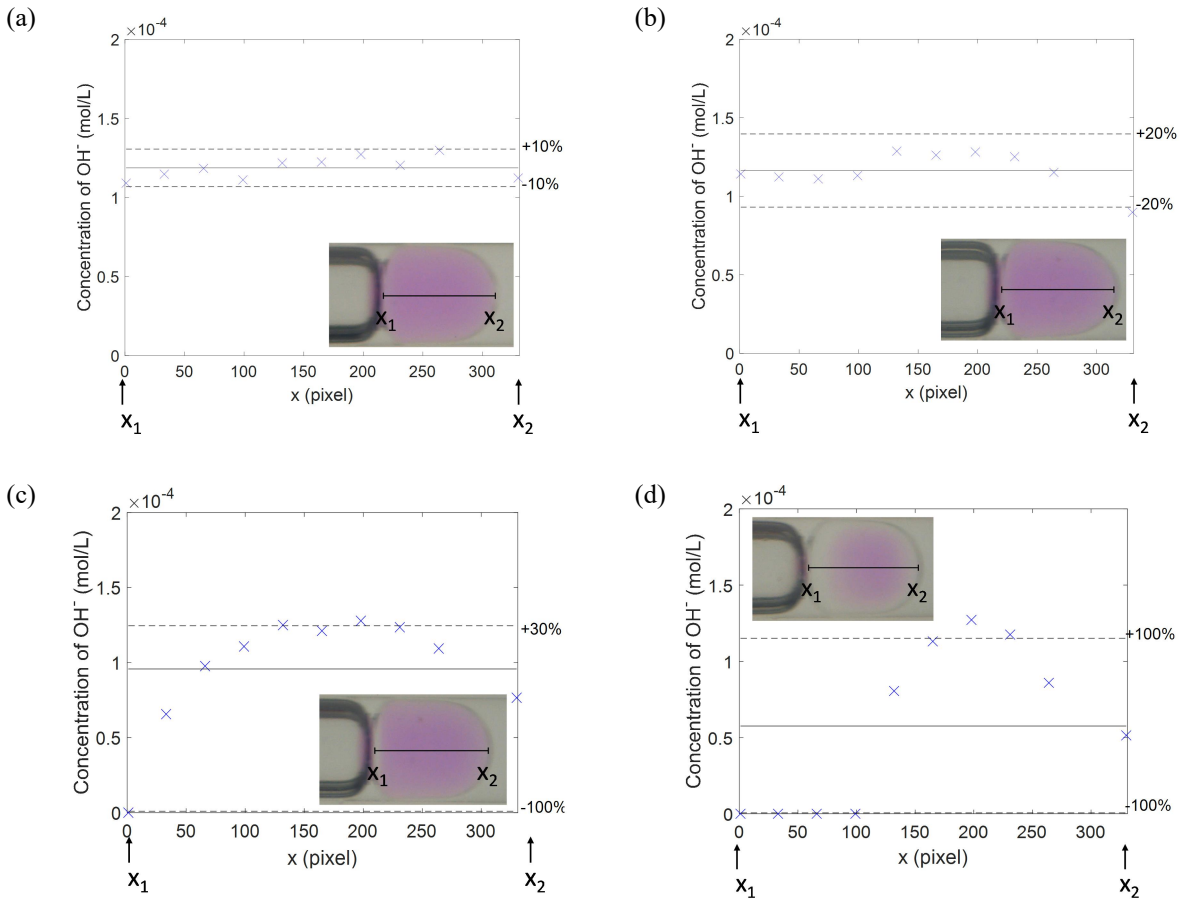

Fig. 9: Verification of concentration homogeneity in the basic droplet for different concentration of acetic acid in the acid droplet, Concentration of OH- along the x axis at the same residence time (a) with C_{AcOH}^0=0.05 M, (b) with C_{AcOH}^0=0.1 M, (c) with C_{AcOH}^0=0.25 M and (d) with C_{AcOH}^0=0.5 M (For the colourless area, the OH^- concentration is approximated to 0).

ease with which the acetic acid is transported from the aqueous acid droplet to the basic droplet, is introduced.

Assuming that AcOH mass transport at the aqueous side of the interface is not limiting, the global concentration gradient is defined as the maximal AcOH concentration in the squalane phase ($\sim C_{AcOH}^{0}/K$ where K is the partition coefficient) minus the AcOH concentration in the basic droplet. Under the assumption that the acetic acid is instantaneously neutralized in the basic droplet, $C_{aq1} = 0$, K_{eff} is defined as:

$$K_{eff} = \frac{K}{C_{AcOH}{}^{0}} r_{AcOH} \qquad (3)$$

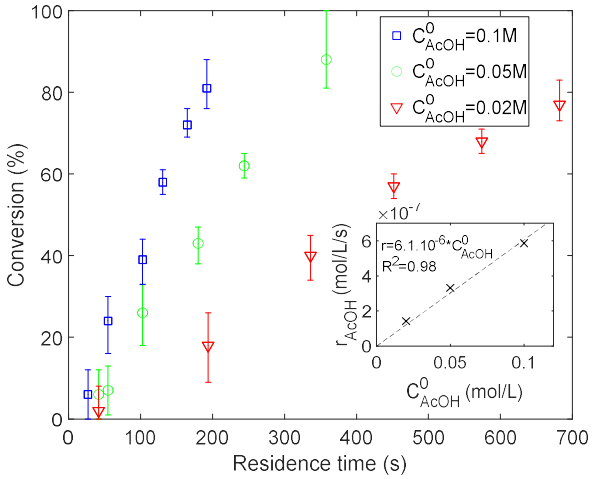

Fig. 10: Evolution of the conversion X along the reactor at different initial concentrations of acetic acid in the acid droplet and global mass transport rate of acetic acid r_{AcOH} as a function of the initial concentration of acetic acid.

The global conductance K_{eff} can be calculated from the slope of the curve presented in Fig. 10 and amounts $1.4 \cdot 10^{-2}$ s^{-1}. It is important to underline that the global conductance is the result of several processes in series and in parallel. These considerations will be further discussed in the next section.

As already discussed, for $C_{AcOH}{}^{0}$ larger than 0.1M, the OH^- concentration was not homogeneous inside the basic droplet and the experiments cannot be directly compared because they seem to be in another

physical regime. The gradient observed inside the basic droplet may indicate a transport limitation due to a relative poor droplet mixing. The mixing inside a droplet flowing through a straight channel has been investigated [29]. When the convection is fast compared to the diffusion, the characteristic mixing time, $t_{mix,d}$, can be estimated as:

$$t_{mix,d} = \frac{d^2}{D} \cdot \left(\frac{0.3}{f_d} + 0.008\right) \tag{4}$$

Where D is the diffusion coefficient and f_d is defined as:

$$f_d = \frac{Ud^2}{L_d D \pi^2} \tag{5}$$

According to the authors, the convection is fast compared to the diffusion if the characteristic time for convection t_{conv} is small compared to the characteristic time for diffusion t_{diff}. The equations for t_{conv} and t_{diff} are presented in Equations (6) and (7) respectively with their order of magnitude for our system. Considering that $t_{conv} << t_{diff}$, Equation (4) can be used for our system and therefore the mixing time in the basic droplet has an order of magnitude of 20 s for all our experiments.

$$t_{conv} = \frac{L_d}{U} \sim 0.1s \tag{6}$$

$$t_{diff} = \frac{d^2}{\pi^2 D} \sim 260s \tag{7}$$

Under the assumption that the acetic acid will be transported in a similar manner compared to the experiments with low C_{AcOH}^0, the acetic acid transport rate can be extrapolated from Equation (3) using the global conductance K_{eff}. To understand why a gradient is observed in experiments using high C_{AcOH}^0, the ratio R is introduced as:

$$R = \frac{\text{quantity of AcOH transferred in 20s}}{\text{quantity of AcOH necessary to discolour the entire droplet}} \cdot 100 \tag{8}$$

R has been calculated for all experiments (see ESI). For C_{AcOH}^{0}=0.5M, the amount of acetic acid transferred in the basic droplet in 20s is equal to 51% of the amount of acetic acid necessary to discolour the entire droplet. In this case, it can be assumed that the transfer rate of acetic acid is too high compared to the mixing rate leading to colourless border. For C_{AcOH}^{0}=0.1M, R is equal to 10% and in this case, no gradient is observed.

Furthermore, due to the formation of dimer at high concentration [30], [31], the partition coefficient of acetic acid between water and squalane, $K=C_{aq}^{*}/C_{org}^{*}$, is lower at high concentration (K=80 for C_{AcOH}^{0}=0.5M and K~2300 for C_{AcOH}^{0}<0.1M). More details on the partition coefficient are given in the ESI. The transport of acetic acid is therefore probably faster at high concentration of acetic acid.

3.2.2. Model for mass transport in alternated segmented flow

A schematic illustration of the unit cell is presented in Fig.11. Unlike the unit cell for typical two-phase segmented flow which contains only one dispersed droplet and one continuous slug, the unit cell for alternated segmented flow is more complex. It can be divided in two parts on each side of the basic droplet (downstream and upstream parts). All the elementary transport processes that can play a role in the acetic acid transport from the acid droplet (aq2) to the basic droplet (aq1) are identified in Fig. 11. Potentially, several parallel processes, each being itself composed of elementary processes in series, could transport acetic acid to the basic droplet. For example, in the downstream part of the unit cell, a potential transport process could go through the gas bubble (1→2→3→4→5→6→7) or could pass through the liquid film (1→13→19→20→16→7) or even could pass through the gas bubble and then through the film (1→2→3→4→5→15→19→20→16→7). Considering the complexity of all the possible transport processes, the strategy was to simplify by removing some elementary transport processes than can either be neglected or because they are not limiting the AcOH transport.

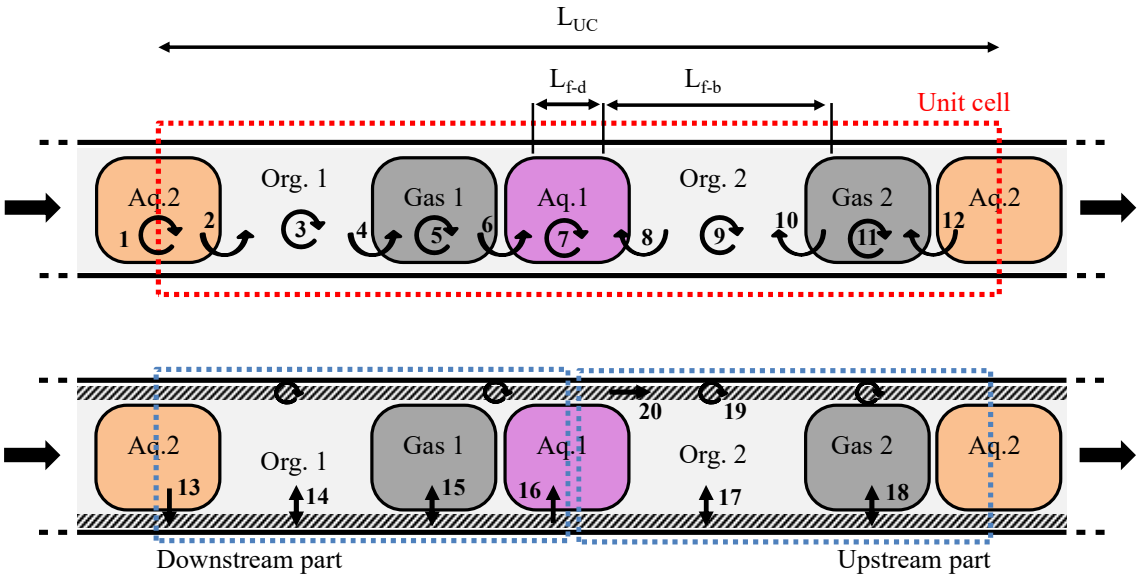

1	Mixing inside the acid droplet
2	Transfer from the acid droplet to the organic slug 1
3	Mixing inside the organic slug 1
4	Transfer from the organic slug 1 to the gas bubble 1
5	Mixing inside the gas bubble 1
6	Transfer from the gas bubble 1 to the basic droplet (separated by a thin squalane film)
7	Mixing inside the basic droplet
8	Transfer from the organic slug 2 to the basic droplet
9	Mixing inside the organic slug 2
10	Transfer from the gas bubble 2 to the organic slug 2
11	Mixing inside the gas bubble 2
12	Transfer from the acid droplet to the gas bubble 2 (separated by a thin squalane film)
13	Transfer between the acid droplet and the film
14	Transport between the organic slug 1 and the film
15	Transfer between the gas bubble 1 and the film
16	Transfer from the film to the basic droplet
17	Transport between the organic slug 2 and the film
18	Transfer between the gas bubble 2 and the film
19	Radial mixing inside the film
20	Axial mixing inside the film

Fig.11: Schematic illustration of the unit cell. Summary of the transport processes in the unit cell for the transport of acetic acid from the acid droplet to the basic droplet.

First, to estimate if the gas bubble can contribute significantly to the transport, a model was build considering only the transport process through the bubble without contribution of the film (1→2→3→4→5→6→7 and 12→11→10→9→8→7). We found that the calculated global conductance (K_{eff}=$10^{-11}s^{-1}$) is extremely low compared to the experimental results (K_{eff}=$10^{-2}s^{-1}$). More details on the transport through the gas bubbles can be found in the ESI. The assumption was made therefore that all of the acetic acid was transported by the liquid film and thus transport processes 4, 5,

6, 10, 11, 12, 15 and 18 were not taken into account in the modelling approach. In other words, we assume that the gas bubble acts as a hermetic barrier between the two aqueous droplets.

To simplify further the modelling approach, characteristic times for the remaining elementary processes were evaluated (see Table 3). The diffusion coefficient D of acetic acid in squalane was estimated at 6.10^{-11} m/s [32]. Given that the global transport process results from several elementary processes in series and in parallel, the strategy is to look at elementary processes in series and eliminates the one that are not limiting the mass transfer. For example, considering the transport process 1→2→3→14→16, the mixing inside the slug is assumed to be really fast and given that $t_{caps} >> t_{mix,s}$, we assume that transports 3 and 9 do not limit the acetic acid transport. Furthermore, $t_{caps} > t_{mix,d}$ and as discussed in the previous section, at low initial acid concentration (⩽0.1M), the concentration of OH^- was homogeneous in the droplet. Therefore we assume that transports 1 and 7 do not limit the AcOH transport. The characteristic for the overall AcOH transport can be calculated from experimental data ($t_{eff}=1/K_{eff}$) and is estimated at 75 s. This value is consistent with the characteristic time for transports at the interface ($t_{f\text{-}d}$ and t_{caps}).

Table 3: Estimation of characteristic times for the elementary transport processes.

Transport processes	Characteristic time	Ref.	Order of magnitude for our system
1, 7	$t_{mix,d} = \frac{d^2}{D} \cdot (\frac{0.3}{f_d} + 0.008)$	[26]	20 s
3, 9	$t_{mix,s} = 3 \cdot \frac{L_s}{U}$	[33]	0.5 s
2, 8	$t_{caps} = \frac{1}{k_{caps} a_{caps}} = \frac{\pi}{\sqrt{2}} \sqrt{\frac{d}{DU}} \frac{L_{UC}}{4}$	[34]	250 s
13, 16	$t_{f-d} = \frac{1}{k_{f-d} a_{f-d}} = \frac{\sqrt{\pi}}{2} \sqrt{\frac{L_{f-d}}{DU}} \frac{dL_{UC}}{4L_{f-d}}$	[34]	100 s
14, 17	$t_{f-s} = \frac{1}{k_{f-s} a_{f-s}} = \frac{d}{3.66D} \frac{dL_{UC}}{4L_{f-s}}$	[35]	10 000 s
19	$t_{mix\ rad,f} = \frac{\delta^2}{D}$		30 s
20	$t_{mix\ ax,f} = \frac{{L_{UC}}^2}{D}$		10^6 s
Global AcOH transport	$t_{eff} = \frac{1}{K_{eff}}$		75 s

For transport processes in the liquid film, it is important to note that the velocity in the film is quite different from the velocity of the dispersed slugs. Howard et Walsh [36] have reported that the velocity profile in the film is parabolic and depends mostly on the viscosity ratio between the dispersed and the continuous phases. They found out that a rough estimation of the velocity profile in the film along radial axis r can be given by:

$$U_{film}(r) = \frac{2U}{1 + \frac{R_d}{R}\left(\frac{\mu_{film}}{\mu_d} - 1\right)}\left(1 - \frac{r^2}{R^2}\right) \quad (9)$$

Using Eq. (9), the maximum velocity in the liquid can be roughly estimated at around 0.1 mm/s. Considering that total superficial velocity of the flow U is significantly superior to the maximum velocity of the film (U~10 mm/s) and to simplify the modelling approach to a simple asymptotic one, the organic film is supposed to be stagnant in the model. The axial and radial mixing inside the film (transports 19 and 20) happened therefore mainly by diffusion. The axial mixing inside the film characterized by $t_{mix\ ax,f}$ is really slow and therefore can be neglected. The radial mixing characterized by $t_{mix\ rad,f}$ is relatively fast and therefore we assume that for a small slice dx of reactor, the acetic acid concentration is constant in the liquid film. Furthermore, considering that the Fourier number Fo<<1 (Fo~10^{-3}), the liquid film is not saturated [37], [38].

To sum up, only the transport processes represented in Fig. 12 are taken into account in the modelling approach. Under the assumption of a stagnant liquid film, the dispersed phases flow through a section with a reduced diameter that takes into account the thickness of the film. The film thickness has been estimated by the well-established correlation of Aussillous and Quéré [39]:

$$\frac{\delta}{R} = \frac{1.34Ca^{2/3}}{1 + 3.35Ca^{2/3}} = 30 - 50\mu m \quad (10)$$

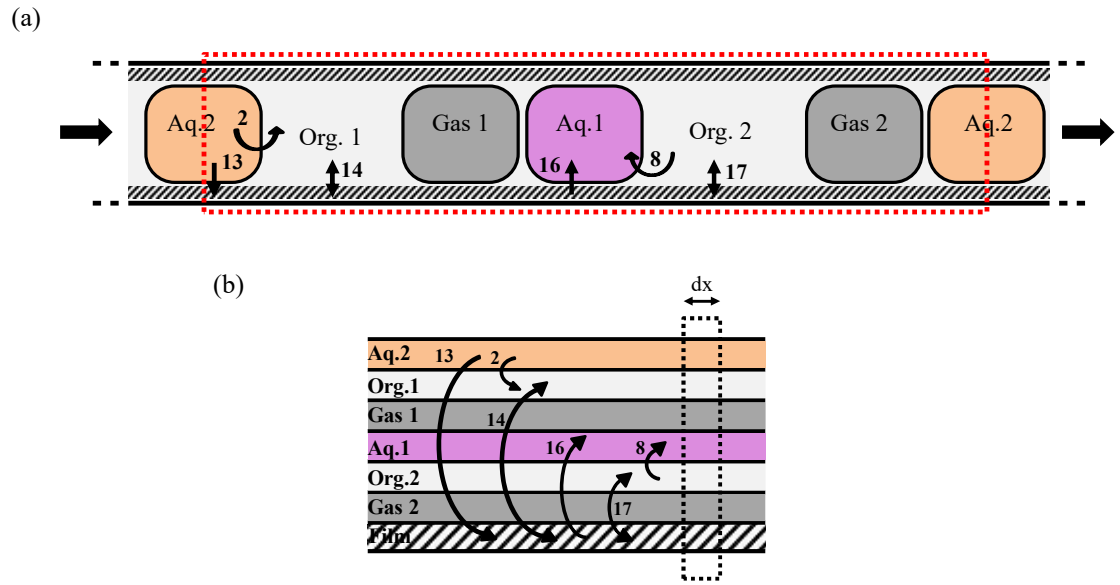

Fig.12: (a) Schematic illustration of the unit cell with the transport processes of interest for the model, (b) Schematic illustration for the plug flow steady state modelling approach.

The transfer 2 between the acid droplet (Aq. 2) and the organic slug 1 and the transfer 8 between the organic slug 2 and the basic droplet (Aq. 1) operate via the same mass transfer coefficient k_{caps}. Under the assumption that the droplet caps are half spheres, the interfacial area for transfer 2 and 8, a_{caps}, is equal to:

$$a_{caps} \approx \frac{2}{L_{UC}} \tag{11}$$

Transports 13 and 16 are assumed to operate via the same transfer coefficient $k_{f\text{-}d}$. The interfacial areas for transfer 13 and 16 are calculated as:

$$a_{f-d} \approx \frac{4L_{f-d}}{dL_{UC}} \tag{12}$$

For the mass exchange between the slug and the liquid film (transports 14 and 17), the literature analysis of fully-developed laminar flow in a circular channel with a constant boundary concentration

was used with the assumption of the limiting constant value of the Sherwood number (Sh = 3.66) [35]. Therefore, transports 14 and 17 are assumed to operate via the same transfer coefficient $k_{f\text{-}s}$ which is calculated as:

$$k_{f-s} = \frac{3.66D}{d} \tag{13}$$

The characteristic time for processes 14 and 17 are surprisingly high compared to that of processes 13 and 16, which could be considered analogous. The application of the correlation set for a monophasic liquid flow in a capillary (Eq. 13) to the case of segmented (Taylor) flow could be questionable but was proposed in previous work.[35] Maybe, the characteristic length used in the original work does not apply here. The transfer between the slug and the film has been artificially increased by changing the characteristic length in the correlation (Eq 13) from the channel diameter to the film thickness. This sensitivity analysis did not change the conclusion about the predominant path through the film for the AcOH transport. More details on this topic are available in the ESI.

For transport 14 and 17, the interfacial areas are estimated as:

$$a_{f-s} \approx \frac{4L_{f-s}}{dL_{UC}} \tag{14}$$

Under the assumption that the acetic acid is instantaneously neutralized by OH^- , the mass balance in each phase was established at steady state in a small reactor slice dx and results in the system of algebro-differential equations presented in Table 4. The concentration of acetic acid in each phase is assumed to be constant in the small reactor slice dx. The partition coefficient K is assumed to be constant (K=2300) for $C_{AcOH}^{0} \leqslant 0.1M$. The length of the unit cell is assumed to stay constant at all residence time (the expansion of the bubble length due to pressure drop can be neglected). To verify this hypothesis, measurements of the bubble length variation reveals a maximum length increase of 12% which could be considered as negligible (See ESI).

One experiment was made without adding gas bubble as separator. The unit cell is therefore modified (see Fig.13). The model is adjusted by adding two transports between the organic slug 1 and the basic

droplet (transport 21) and between the acid droplet and the organic slug 2 (transport 22). The adjusted system of algebra-differential equations is given in Table 5.

Table 4: System of algebro-differential equations for the alternated segmented flow with gas bubbles.

Phase	Equations	
Aq. 2	$\varepsilon_{aq2} U \frac{dC_{aq2}}{dx} = -k_{caps} a_{caps} \cdot \left(\frac{C_{aq2}}{K} - C_{org1}\right) - k_{f-d} a_{f-d} \cdot \left(\frac{C_{aq2}}{K} - C_{film}\right)$	(15)
Org. 1	$\varepsilon_{org1} U \frac{dC_{org1}}{dx} = k_{caps} a_{caps} \cdot \left(\frac{C_{aq2}}{K} - C_{org1}\right) - k_{f-s} a_{f-s} (C_{org1} - C_{film})$	(16)
Aq. 1	$\varepsilon_{aq1} U \frac{dC_{aq1}}{dx} = k_{caps} a_{caps} \cdot (C_{org2} - 0) + k_{f-d} a_{f-d} \cdot (C_{film} - 0)$	(17)
Org. 2	$\varepsilon_{org2} U \frac{dC_{org2}}{dx} = -k_{caps} a_{caps} \cdot (C_{org2} - 0) - k_{f-s} a_{f-s} (C_{org2} - C_{film})$	(18)
Film	$0 = k_{f-d} a_{f-d} \cdot \left(\frac{C_{aq2}}{K} - C_{film}\right) + k_{f-s} a_{f-s} (C_{org1} - C_{film}) - k_{f-d} a_{f-d} \cdot (C_{film} - 0) + k_{f-s} a_{f-s} (C_{org2} - C_{film})$	(19)

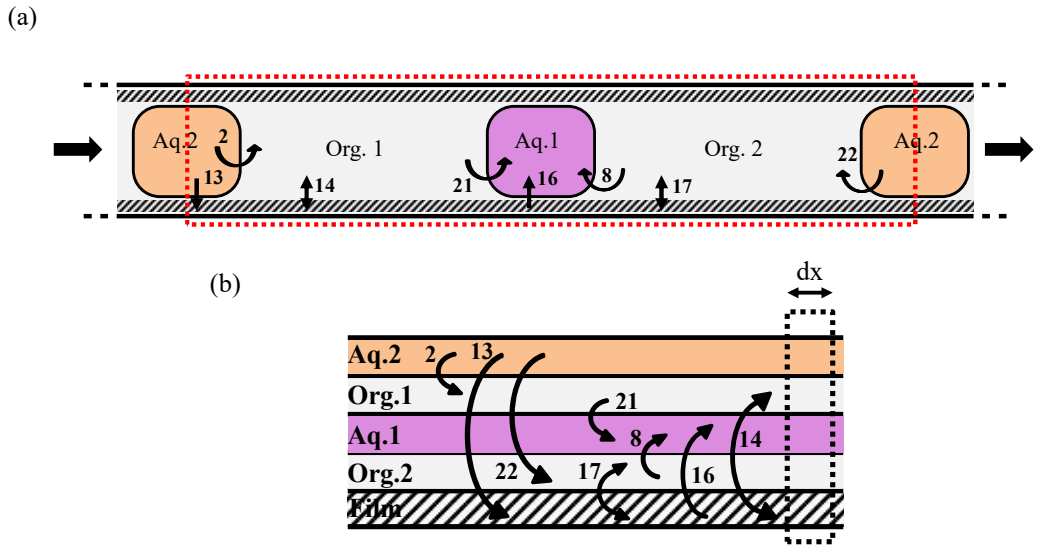

Fig.13: (a) Schematic illustration of the unit cell without gas with the transport processes of interest for the model, (b) Schematic illustration for the plug flow steady state modelling approach.

Table 5: System of algebro-differential equations for the alternated segmented flow without gas bubbles.

Phase	Equations	
Aq. 2	$\varepsilon_{aq2} U \frac{dC_{aq2}}{dx} = -k_{caps} a_{caps} \cdot \left(\frac{C_{aq2}}{K} - C_{org1}\right) - k_{caps} a_{caps} \cdot \left(\frac{C_{aq2}}{K} - C_{org2}\right) - k_{f-d} a_{f-d} \cdot \left(\frac{C_{aq2}}{K} - C_{film}\right)$	***(20)***
Org. 1	$\varepsilon_{org1} U \frac{dC_{org1}}{dx} = k_{caps} a_{caps} \cdot \left(\frac{C_{aq2}}{K} - C_{org1}\right) - k_{f-s} a_{f-s} \left(C_{org1} - C_{film}\right) - k_{caps} a_{caps} \cdot \left(C_{org1} - 0\right)$	***(21)***
Aq. 1	$\varepsilon_{aq1} U \frac{dC_{aq1}}{dx} = k_{caps} a_{caps} \cdot \left(C_{org2} - 0\right) + k_{f-d} a_{f-d} \cdot \left(C_{film} - 0\right) + k_{caps} a_{caps} \cdot \left(C_{org1} - 0\right)$	***(22)***
Org. 2	$\varepsilon_{org2} U \frac{dC_{org2}}{dx} = -k_{caps} a_{caps} \cdot \left(C_{org2} - 0\right) - k_{f-s} a_{f-s} (C_{org2} - C_{film}) + k_{caps} a_{caps} \cdot \left(\frac{C_{aq2}}{K} - C_{org2}\right)$	***(23)***
Film	$0 = k_{f-d} a_{f-d} \cdot \left(\frac{C_{aq2}}{K} - C_{film}\right) + k_{f-s} a_{f-s} \left(C_{org1} - C_{film}\right) - k_{f-d} a_{f-d} \cdot \left(C_{film} - 0\right) + k_{f-s} a_{f-s} (C_{org2} - C_{film})$	***(24)***

3.2.3. Comparison of AcOH transport with and without gas

At the same flow rates (Q_{aq1}=0.24mL/min, Q_{aq2}=0.24 mL/min and $Q_{squalane}$=0.6 mL/min), two experiments were made with either an addition of gas (Q_{gas}=0.6 ml/min) or an addition of more squalane ($Q_{squalane}$=0.6 mL/min) at the T-junction. Therefore, the gas bubbles are replaced in the experiment without gas by the same amount of squalane (see Fig. 14). The length of the unit cell is the same for both experiments. For the experiment without gas bubbles, the conversion can be measured only for small residence time (t<100s) because of the quite fast coalescence of the two aqueous droplets when there is no gas bubble acting as separator.

The comparison between the experiments with and without gas (see Fig. 14 (b)) indicates that the gas bubble act effectively as an obstacle to the acetic acid transport by limiting the transport from the squalane slug to the basic droplet. In the model with gas bubble, the parameter k_{caps} doesn't play a significant role in the acetic acid transfer because the majority of the transfer happened via transports 13 and 16. Using the modelling approach, $k_{f\text{-}d}$ was adjusted to fit the experiment with gas bubble and thereafter by keeping $k_{f\text{-}d}$ fixed, k_{caps} was adjusted using the experiment without gas. $k_{f\text{-}d}$ and k_{caps} were respectively equal to $1.4 \cdot 10^{-5}$ and $1.15 \cdot 10^{-5}$ m/s. To compare the mass transfer coefficient obtained in this work with the literature, we use the correlation of Van Baten and Khrishna [34] which separates the caps and film contribution. Using the correlation, $k_{f\text{-}d}$ and k_{caps} were estimated respectively at $2.6 \cdot 10^{-5}$ m/s and $2.1 \cdot 10^{-5}$ m/s which is the same order of magnitude we obtained.

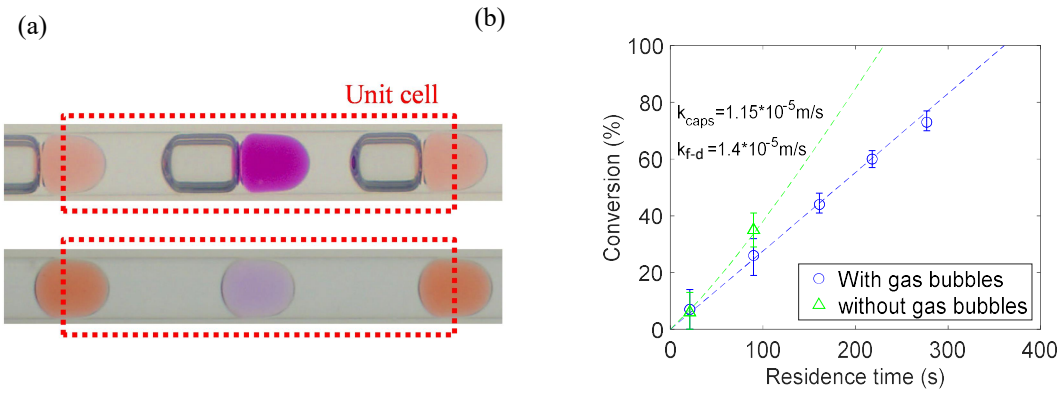

Fig.14: (a) Photos of the unit cell for the experiment with and without gas bubbles. The colour difference between the two pictures is not representative of what happened in the experiment (the pictures were taken during hydrodynamic tests). (b) Experimental conversion and modelling results.

3.2.4. Influence of superficial velocity

Experiments were made at different superficial velocities U ranging from 7 mm/s to 18.6 mm/s. The configuration of the unit cell (droplets, slugs and bubbles lengths) was kept approximately constant for all experiments by keeping the ratios $Q_{aq1}/(Q_{aq1}+ Q_{aq2}+ Q_{squalane})$ and $Q_{gas}/Q_{squalane}$ constant. Using the modelling approach, $k_{f\text{-}d}$ was varied to fit the experimental data while keeping the ratio $k_{caps}/k_{f\text{-}d}$ equal to the same value as determined in the previous part. Fig. 15 shows the influence of the superficial

velocity on k_{caps} and k_{f-d}. An increase of the superficial velocity U leads to slight increase of the mass transfer coefficients k_{caps} and k_{f-d} which agrees with the correlation of Van Baten and Khrishna [34].

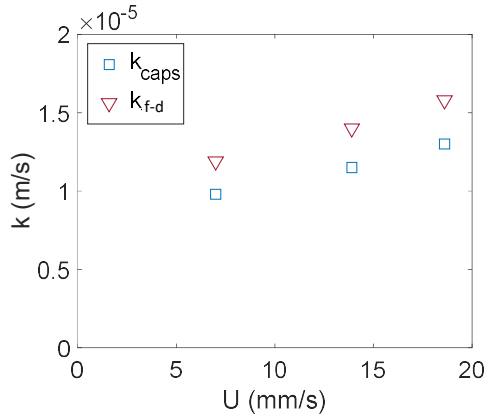

Fig.15: Influence of superficial velocity on the mass transfer coefficient k_{caps} and k_{f-d}

3.2.5. Influence of gas bubble length

Experiments were made to look at the influence of the bubble length on the mass transfer. For all experiments, the ratio $Q_{aq1}/(Q_{aq1}+ Q_{aq2}+ Q_{squalane})$ was kept constant and thus the configuration of the flow pattern that comes out of the first cross mixer was approximately the same (same droplet and slug lengths). The flow rate of gas added at the T junction is varied so that the bubble length and the unit cell increase (see Fig. 16 (a)). The superficial velocity varies slightly (from 12.6 to 14.9 mm/s) but this

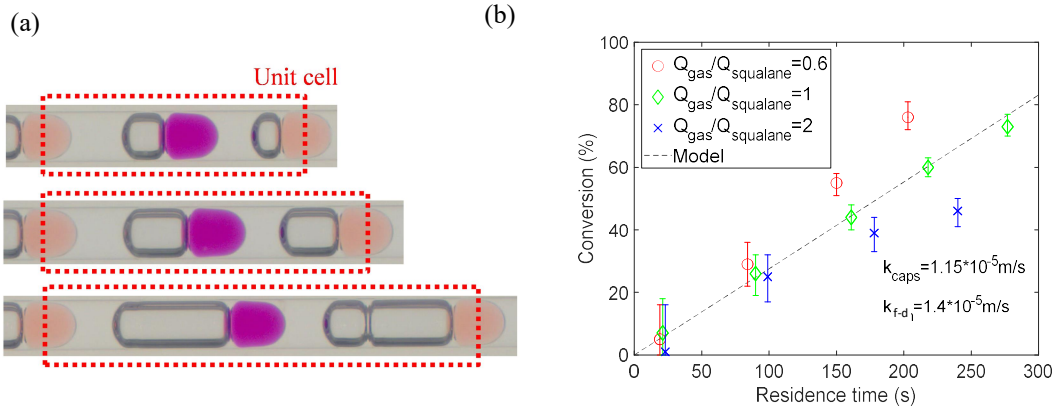

Fig.16: (a) Photos of the unit cell for the experiments on the gas influence, from top to bottom $Q_{gas}/Q_{squalane}$=0.6, $Q_{gas}/Q_{squalane}$ =1, $Q_{gas}/Q_{squalane}$ =2, (b) Experimental conversion and results from the simulation.

small variation is not expected to impact significantly the transport of AcOH as shown in the precedent section. As shown in Fig. 16 (b), for the same residence time, when the bubble length increases, the conversion slightly decreases. The simulation was made by keeping $k_{f\text{-}d}$ and k_{caps} fixed ($k_{f\text{-}d}$ =1.4·10^{-5} and k_{caps}=1.15·10^{-5} m/s). The modelling approach doesn't capture the slight influence of the gas bubble length. Indeed, the experimental data for $Q_{gas}/Q_{squalane}$=0.6 are superior to the one calculated by the model and the experimental data for $Q_{gas}/Q_{squalane}$ =2 are generally inferior to the one calculated by the model (see Fig. 16).

Some of the assumptions made in the modelling approach are perhaps too drastic to describe precisely the effect of the bubble length. To go further, a more precise and detailed modelling approach using Computational Fluid Dynamics (CFD) could be used to investigate locally what is happening in the squalane film. The transport in ASF has been so far seldom studied. Asano et al. [24] have reported qualitative observations on the transport in ASF (without gas) with very long droplets (L_d>1cm). They observed a concentration gradient between the front and rear caps of the receiving droplet and proposed a transfer mechanism where the film plays an important role in the solute transport. The asymmetric behaviour is not observed in our work which can be explained by the large difference in droplet length. However our work also points out the large contribution of the liquid film.

4. Conclusions

In this work, we have investigated the hydrodynamics and mass transfer of the alternated segmented flow. Concerning the hydrodynamics, we were able using a simple system without active control (i.e. valves) to generate the ASF and more importantly for the first time, to keep the ASF stable for long residence time by adding gas bubbles that acts as separator between the miscible droplets. Different flow regimes were identified (i.e. coalescence, ASF with small droplet, ASF) and the operating window was characterized by cartography. A first look at the influence of the fluid properties (i.e. viscosities of the continuous and dispersed phase and surface tension between the continuous and

dispersed phase) was proposed. The formation of ASF was possible for viscous continuous phase ($\geqslant$19cP) and with a surface tension greater than 30 mN/m. While the range of operating conditions may look rather limited, it is believed it could easily be extended to higher pressures and longer residence times. In addition, a broader range of hold-up for the fluid phases, such as the gas phase for hydrogenation reactions, could be achieved using different injectors as already reported [40].

Concerning the mass transfer study, we have developed a colorimetric method to evaluate the efficiency of the transport between the two droplets. The comparison between the experiment with and without gas shows that the gas bubble limits the transport of solute but this limitation is not very large because the liquid film plays an important role in the solute transport. A modelling approach that differentiate the film and caps contribution in the unit cell was proposed and $k_{f\text{-}d}$ and k_{caps} were evaluated respectively as $1.4 \cdot 10^{-5}$ and $1.15 \cdot 10^{-5}$ m/s which agrees with the order of magnitude given by the correlation of Van Baten and Khrishna [34]. A slight increase of $k_{f\text{-}d}$ and k_{caps} was observed with an increase in the superficial velocity. Furthermore, when the bubble length increases, the solute transport rate slightly decreases. This slight tendency is not captured by the model and more precise modelling approach like CFD could be used to describe more accurately what is happening in the liquid film.

5. Acknowledgments

The authors kindly acknowledge funding by the H2020-FET-Open programme of the European Commission (grant no. 737266 project H2020 FET-OPEN ONE-FLOW), co-funding by CNRS (UMR5285), CPE Lyon for hosting the experimental work and Dr. Youssef Swesi for fruitful discussions on the modelling work.

Nomenclature

a	Interfacial area per unit cell of volume (m^2/m^3)
C	Concentration (mol/L)
d	Channel diameter (m)
D	Diffusion coefficient of acetic acid (m^2/s)
k	Mass transfer coefficient (m/s)
K	Partition coefficient of AcOH, $K = \frac{C_{aq}^*}{C_{org}^*}$
K_{eff}	Global conductance characterizing AcOH transport (s^{-1})
L	Length (m)
Q	Flow rate (mL/min)
R	Channel radius (m)
R_d	Droplet radius (m), $R_d = R - \delta$
U	Total superficial velocity (m/s)
U_{film}	Film velocity (m/s)
$t_{mix,d}$	Characteristic mixing time inside a droplet (s)
t_{diff}	Characteristic time for diffusion (s)
t_{conv}	Characteristic time for convection (s)
$t_{mix,s}$	Characteristic mixing time inside a slug (s)
$t_{mix,rad,f}$	Characteristic radial mixing time in the film (s)
$t_{mix,ax,f}$	Characteristic axial mixing time in the film (s)
V	Volume (m^3)
r_{AcOH}	Global transport rate of acetic acid (mol of AcOH/L of basic aq. phase/s)
Ca	Capillary number, $Ca = \frac{U\mu_{squalane}}{\gamma}$
Re	Reynolds number, $Re = \frac{\rho_{squalane} U d}{\mu_{squalane}}$
Fo	Fourier number, $= \frac{DL_{f-d}}{U\delta^2}$
aq	refers to all the aqueous phase (aq1 + aq2)
aq 1	refers to the blue droplet (hydrodynamics) or the basic droplet (mass transfer)
aq 2	refers to the red droplet (hydrodynamic) or the acid droplet (mass transfer)
AcOH	refers to the acetic acid
OH^-	refers to the hydroxide ion

References

[1] A. Cybulski† and J. A. Moulijn, "Structured Reactors, a Wealth of Opportunities," in *Novel Concepts in Catalysis and Chemical Reactors*, John Wiley & Sons, Ltd, 2010, pp. 189–209.

[2] M. N. Kashid and L. Kiwi-Minsker, "Microstructured Reactors for Multiphase Reactions: State of the Art," *Ind. Eng. Chem. Res.*, vol. 48, no. 14, pp. 6465–6485, Jul. 2009, doi: 10.1021/ie8017912.

[3] S. Haase, D. Y. Murzin, and T. Salmi, "Review on hydrodynamics and mass transfer in minichannel wall reactors with gas–liquid Taylor flow," *Chem. Eng. Res. Des.*, vol. 113, pp. 304–329, Sep. 2016, doi: 10.1016/j.cherd.2016.06.017.

[4] J. Tan, C. Dong, Y. C. Lu, J. H. Xu, and G. S. Luo, "Coupling Process of Oxidation and Extraction in a Gas–Liquid–Liquid Microdispersion System for H2O2 Synthesis," *Ind. Eng. Chem. Res.*, vol. 51, no. 4, pp. 1834–1845, Feb. 2012, doi: 10.1021/ie2010302.

[5] D. Karan and S. A. Khan, "Mesoscale triphasic flow reactors for metal catalyzed gas–liquid reactions," *React. Chem. Eng.*, vol. 4, no. 7, pp. 1331–1340, Jun. 2019, doi: 10.1039/C9RE00150F.

[6] S. K. Yap *et al.*, "Rapid nanoparticle-catalyzed hydrogenations in triphasic millireactors with facile catalyst recovery," *Green Chem.*, vol. 16, no. 11, pp. 4654–4658, Oct. 2014, doi: 10.1039/C4GC01504E.

[7] A.-K. Liedtke, F. Bornette, R. Philippe, and C. de Bellefon, "Gas–liquid–solid 'slurry Taylor' flow: Experimental evaluation through the catalytic hydrogenation of 3-methyl-1-pentyn-3-ol," *Chem. Eng. J.*, vol. 227, pp. 174–181, Jul. 2013, doi: 10.1016/j.cej.2012.07.100.

[8] T. Horie, M. Sumino, T. Tanaka, Y. Matsushita, T. Ichimura, and J. Yoshida, "Photodimerization of Maleic Anhydride in a Microreactor Without Clogging," *Org. Process Res. Dev.*, vol. 14, no. 2, pp. 405–410, Mar. 2010, doi: 10.1021/op900306z.

[9] D. I. Enache, G. J. Hutchings, S. H. Taylor, and E. H. Stitt, "The hydrogenation of isophorone to trimethyl cyclohexanone using the downflow single capillary reactor," *Catal. Today*, vol. 105, no. 3, pp. 569–573, Aug. 2005, doi: 10.1016/j.cattod.2005.06.013.

[10] A.-K. Liedtke, F. Bornette, R. Philippe, and C. de Bellefon, "External liquid solid mass transfer for solid particles transported in a milli-channel within a gas–liquid segmented flow," *Chem. Eng. J.*, vol. 287, pp. 92–102, Mar. 2016, doi: 10.1016/j.cej.2015.10.109.

[11] A.-K. Liedtke, F. Scheiff, F. Bornette, R. Philippe, D. W. Agar, and C. de Bellefon, "Liquid–Solid Mass Transfer for Microchannel Suspension Catalysis in Gas–Liquid and Liquid–Liquid Segmented Flow," *Ind. Eng. Chem. Res.*, vol. 54, no. 17, pp. 4699–4708, May 2015, doi: 10.1021/ie504523y.

[12] A. Ufer, M. Mendorf, A. Ghaini, and D. W. Agar, "Liquid/Liquid Slug Flow Capillary Microreactor," *Chem. Eng. Technol.*, vol. 34, no. 3, pp. 353–360, Mar. 2011, doi: 10.1002/ceat.201000334.

[13] K. Olivon and F. Sarrazin, "Heterogeneous reaction with solid catalyst in droplet-flow millifluidic device," *Chem. Eng. J.*, vol. 227, pp. 97–102, Jul. 2013, doi: 10.1016/j.cej.2012.08.098.

[14] M. Frey, L. Violet, D. Richard, and P. Fongarland, "Experimental and CFD study of a new one-pot reactor for hybrid catalysis," *Chem. Eng. J.*, vol. 383, p. 122958, Mar. 2020, doi: 10.1016/j.cej.2019.122958.

[15] V. V. Ordomsky, J. C. Schouten, J. van der Schaaf, and T. A. Nijhuis, "Multilevel rotating foam biphasic reactor for combination of processes in biomass transformation," *Chem. Eng. J.*, vol. 231, pp. 12–17, Sep. 2013, doi: 10.1016/j.cej.2013.06.110.

[16] M. M. E. Delville, K. Koch, J. C. M. van Hest, and F. P. J. T. Rutjes, "Chemoenzymatic flow cascade for the synthesis of protected mandelonitrile derivatives," *Org. Biomol. Chem.*, vol. 13, no. 6, pp. 1634–1638, Jan. 2015, doi: 10.1039/C4OB02128B.

[17] D. Webb and T. F. Jamison, "Continuous flow multi-step organic synthesis," *Chem. Sci.*, vol. 1, no. 6, pp. 675–680, Nov. 2010, doi: 10.1039/C0SC00381F.

[18] A. R. Bogdan, S. L. Poe, D. C. Kubis, S. J. Broadwater, and D. T. McQuade, "The Continuous-Flow Synthesis of Ibuprofen," *Angew. Chem. Int. Ed.*, vol. 48, no. 45, pp. 8547–8550, Oct. 2009, doi: 10.1002/anie.200903055.

[19] H. P. N. Surya, S. Parayil, U. Banerjee, S. Chander, and A. K. Sen, "Alternating and merged droplets in a double T-junction microchannel," *BioChip J.*, vol. 9, no. 1, pp. 16–26, Mar. 2015, doi: 10.1007/s13206-014-9103-1.

[20] B. Zheng, J. D. Tice, and R. F. Ismagilov, "Formation of Droplets of Alternating Composition in Microfluidic Channels and Applications to Indexing of Concentrations in Droplet-Based Assays," *Anal. Chem.*, vol. 76, no. 17, pp. 4977–4982, Sep. 2004, doi: 10.1021/ac0495743.

[21] B.-J. Jin, Y. W. Kim, Y. Lee, and J. Y. Yoo, “Droplet merging in a straight microchannel using droplet size or viscosity difference,” *J. Micromechanics Microengineering*, vol. 20, no. 3, p. 035003, Feb. 2010, doi: 10.1088/0960-1317/20/3/035003.

[22] M. Saqib, O. B. Şahinoğlu, and E. Y. Erdem, “Alternating Droplet Formation by using Tapered Channel Geometry,” *Sci. Rep.*, vol. 8, no. 1, pp. 1–9, Jan. 2018, doi: 10.1038/s41598-018-19966-y.

[23] L. Frenz, J. Blouwolff, A. D. Griffiths, and J.-C. Baret, “Microfluidic Production of Droplet Pairs,” *Langmuir*, vol. 24, no. 20, pp. 12073–12076, Oct. 2008, doi: 10.1021/la801954w.

[24] S. Asano, Y. Takahashi, T. Maki, Y. Muranaka, N. Cherkasov, and K. Mae, “Contactless mass transfer for intra-droplet extraction,” Sci. Rep., vol. 10, no. 1, pp. 1–9, May 2020, doi: 10.1038/s41598-020-64520-4.

[25] M.T. Kreutzer, F. Kapteijn, J.A. Moulijn, B. Anderson, A. Cybulski “Two-phase segmented flow in capillaries and monolith reactors” in the book “Structured Catalysts and Reactors”, A. Cybulski, J.A. Moulijn Eds, Taylor & Francis, 2nd Edition, 2005, chap. 11. ISBN 0-8247-2343-0 (see eq 11.7, pp 402).

[26] H. Liu, C.O. Vandu, R. Krishna, “Hydrodynamics of Taylor Flow in Vertical Capillaries: Flow Regimes, Bubble Rise Velocity, Liquid Slug Length, and Pressure Drop” *Ind. Eng. Chem. Res.* Vol. 44, pp. 4885-4897 , 2005, doi:10.1021/ie049307n

[27] ex38 C. N. Baroud, F. Gallaire, R. Dangla, “Dynamics of microfluidic droplets,” Lab Chip Vol. 10, no. 16, pp 2032-204, 2010, doi: 10.1039/c001191f

[28] D. J. Donahue and F. E. Bartell, “The Boundary Tension at Water-Organic Liquid Interfaces,” *J. Phys. Chem.*, vol. 56, no. 4, pp. 480–484, Apr. 1952, doi: 10.1021/j150496a016.

[29] K. Handique and M. A. Burns, “Mathematical modeling of drop mixing in a slit-type microchannel,” *J. Micromechanics Microengineering*, vol. 11, no. 5, pp. 548–554, Aug. 2001, doi: 10.1088/0960-1317/11/5/316.

[30] Y. Fujii, H. Yamada, and M. Mizuta, “Self-association of acetic acid in some organic solvents,” *J. Phys. Chem.*, vol. 92, no. 23, pp. 6768–6772, Nov. 1988, doi: 10.1021/j100334a054.

[31] Y. Fujii, K. Sobue, and M. Tanaka, “Solvent effect on the dimerization and hydration constant of benzoic acid,” *J. Chem. Soc. Faraday Trans. 1 Phys. Chem. Condens. Phases*, vol. 74, no. 0, pp. 1467–1476, Jan. 1978, doi: 10.1039/F19787401467.

[32] M. T. Tyn and W. F. Calus, “Diffusion coefficients in dilute binary liquid mixtures,” *J. Chem. Eng. Data*, vol. 20, no. 1, pp. 106–109, Jan. 1975, doi: 10.1021/je60064a006.

[33] C. Yao, Y. Zhao, and G. Chen, “Multiphase processes with ionic liquids in microreactors: hydrodynamics, mass transfer and applications,” *Chem. Eng. Sci.*, vol. 189, pp. 340–359, Nov. 2018, doi: 10.1016/j.ces.2018.06.007.

[34] J. M. van Baten and R. Krishna, “CFD simulations of mass transfer from Taylor bubbles rising in circular capillaries,” *Chem. Eng. Sci.*, vol. 59, no. 12, pp. 2535–2545, Jun. 2004, doi: 10.1016/j.ces.2004.03.010.

[35] C. Butler, E. Cid, and A.-M. Billet, “Modelling of mass transfer in Taylor flow: Investigation with the PLIF-I technique,” *Chem. Eng. Res. Des.*, vol. 115, pp. 292–302, Nov. 2016, doi: 10.1016/j.cherd.2016.09.001.

[36] J. A. Howard and P. A. Walsh, “Review and extensions to film thickness and relative bubble drift velocity prediction methods in laminar Taylor or slug flows,” *Int. J. Multiph. Flow*, vol. 55, pp. 32–42, Oct. 2013, doi: 10.1016/j.ijmultiphaseflow.2013.04.005.

[37] M. T. Kreutzer, F. Kapteijn, J. A. Moulijn, and J. J. Heiszwolf, “Multiphase monolith reactors: Chemical reaction engineering of segmented flow in microchannels,” *Chem. Eng. Sci.*, vol. 60, no. 22, pp. 5895–5916, Nov. 2005, doi: 10.1016/j.ces.2005.03.022.

[38] R. Pohorecki, “Effectiveness of interfacial area for mass transfer in two-phase flow in microreactors,” *Chem. Eng. Sci.*, vol. 62, no. 22, pp. 6495–6498, Nov. 2007, doi: 10.1016/j.ces.2007.07.015.

[39] P. Aussillous and D. Quéré, “Quick deposition of a fluid on the wall of a tube,” *Phys. Fluids*, vol. 12, no. 10, pp. 2367–2371, Sep. 2000, doi: 10.1063/1.1289396.

[40] A. Leclerc, R. Philippe, V. Houzelot, D. Schweich, C. de Bellefon, “Gas-liquid Taylor flow in square micro-channels New inlet geometries and interfacial area tuning” *Chem. Eng. J.* vol. 165, no. 1, pp 290-300, Nov. 2010, doi: 10.1016/j.cej.2010.08.021